Producing multi-coloured bunches through beam-induced ionization injection in plasma wakefield accelerator

Cite this article: Vafaei-Najafabadi N *et al*. 2019 Producing multi-coloured bunches through beam-induced ionization injection in plasma wakefield accelerator. *Phil. Trans. R. Soc. A* **377**: 20180184.
http://dx.doi.org/10.1098/rsta.2018.0184

Accepted: 20 March 2019

One contribution of 10 to a Theo Murphy meeting issue 'Directions in particle beam-driven plasma wakefield acceleration'.

Subject Areas:
high energy physics, plasma physics

Keywords:
plasma, accelerators, particle beams, injection, ionization

Author for correspondence:
N. Vafaei-Najafabadi
e-mail:
navid.vafaei-najafabadi@stonybrook.edu

N. Vafaei-Najafabadi[1], L. D. Amorim[1], E. Adli[2], W. An[3], C. I. Clarke[6], C. E. Clayton[3], S. Corde[4], S. Gessner[5], S. Z. Green[6], M. J. Hogan[6], C. Joshi[3], O. Kononenko[4], C. A. Lindstrøm[2], M. Litos[7], W. Lu[8], K. A. Marsh[3], W. B. Mori[3], P. San Miguel Claveria[4], B. O'Shea[6], G. Raj[4], D. Storey[6], G. White[6], Xinlu Xu[3] and V. Yakimenko[6]

[1]Stony Brook University, Stony Brook, NY 11794, USA
[2]University of Oslo, Oslo 0316, Norway
[3]University of California Los Angeles, Los Angeles, CA 90095, USA
[4]LOA, ENSTA ParisTech, CNRS, Ecole Polytechnique, Université Paris-Saclay, Palaiseau 91762, France
[5]CERN, Geneva, Switzerland
[6]SLAC National Accelerator Laboratory, Menlo Park, CA 94025, USA
[7]University of Colorado Boulder, Boulder, CO 80309, USA
[8]Tsinghua University, Beijing 10084, People's Republic of China

NV-N, 0000-0003-2619-1303; EA, 0000-0002-4351-6619; SC, 0000-0002-5015-0387; CAL, 0000-0002-0769-0425; MDL, 0000-0003-2434-8207

This paper discusses the properties of electron beams formed in plasma wakefield accelerators through ionization injection. In particular, the potential for generating a beam composed of co-located multi-colour beamlets is demonstrated in the case where the ionization is initiated by the evolving charge field of the drive beam itself. The physics of the processes of ionization and injection are explored through OSIRIS simulations. Experimental evidence showing similar

features are presented from the data obtained in the E217 experiment at the FACET facility of the SLAC National Laboratory.

This article is part of the Theo Murphy meeting issue 'Directions in particle beam-driven plasma wakefield acceleration'.

1. Introduction

A beam-driven plasma wakefield accelerator (PWFA) uses a highly relativistic, high-density particle beam to drive a nonlinear wave in plasma. Such a wave is generated by the Coulomb force of the drive beam, which pushes the electrons away from the axis of the beam. When the particle beam is dense enough to push all the electrons out, and therefore create a region consisting exclusively of uncovered ions behind it, the interaction regime is known as the blowout regime [1,2]. The heavier ions stay nearly stationary during the interaction and pull the electrons back towards the axis. The fields inside the resulting wave structure (called a wake) can be thousands of times stronger than those of the RF accelerators. Accelerating gradients of up to $50\,\mathrm{GeV\,m^{-1}}$, sustained over a metre of plasma, have been demonstrated using an electron drive beam [3]. Additionally, the efficiency of energy transfer from the drive to a trailing beam placed in the proper, accelerating, phase of the wakefield has reached over 30% [4].

A primary challenge is finding a method for producing and placing a high-quality charge in the accelerating phase of the wake to form the trailing beam and to maintain the quality of this beam during acceleration. Ionization injection [5–8] is one such method for producing the trailing electron beam from the neutral atoms or ions already present in the wakefield. In this process, a high-ionization-threshold (HIT) impurity element is added at low concentration to a low-ionization-threshold (LIT) gas. The LIT gas is ionized by the front edge of the drive beam or by an external source such as a laser and serves as the main plasma source. The wake is then excited by the bulk of the beam in this plasma. The HIT impurity, on the other hand, is ionized only within the wakefield. The electrons resulting from the ionization of the HIT element gain energy from the wakefield as they slip backwards in the frame of the beam. In this process, they can gain sufficient energy from the wake to get trapped and form a trailing beam.

The ionization process may be triggered via the field of one or more laser pulses [9,10], the fields of the wake [11], or the drive electron beam itself [5,6,12]. Simulations have shown that a trailing beam produced via ionization injection can possess a number of desirable properties, including high brightness [9–11]. The focus of the present paper is on the properties of a beam resulting from ionization injection initiated via fields of the drive beam itself, a process known as beam-induced ionization injection (B-III). In particular, we use simulations to demonstrate the possibility of generating a multi-coloured electron bunch, where several distinct electron bunches with different peak energy levels and with narrow energy spread are accelerated in the same location of the wakefield.

Although several other methods have been proposed for creating multiple beams in a plasma wakefield accelerator driven in the blowout regime [13,14], this is the first study of a multi-coloured bunch produced in PWFA that is accompanied by supporting experimental results. The method proposed here has several advantages over the other methods. First, the process of ionization injection in the B-III method is initiated by the fields of the drive beam and therefore does not rely on a separate 'trigger', such as a laser pulse [13,14]. This results in a significantly simpler experimental configuration. For the same reason, the axis of the injected trailing beam is self-aligned with the driver, which avoids potential transverse instabilities that can arise due to the transverse misalignment of the trigger and the drive beam. Second, as will be shown in §3, the distinct beamlets of the multi-coloured bunch produced via the B-III method are injected at the same phase in the wakefield provided that the LIT density is uniform. This results in the beamlets experiencing the same accelerating field, and maintaining their relative energy separation during the acceleration process. For this reason, using B-III allows the creation of a multi-coloured beam

with prescribed energy separation, which is decoupled from its desired final energy. Finally, the control of the length and profile of the HIT section allows control over the number of beamlets, and their desired relative charge distribution.

This beam enables simultaneous probing of a phenomenon using an electron beam with two distinct energies. Moreover, using standard techniques such as that used in [15], they can be separated to any delay on micron scale and be of potential use for creating multi-colour radiation in a Free Electron Laser. The rest of this paper is organized as follows: the physical processes that underlie B-III are described in §2. In §3, we will describe how this process can be used to generate a multi-colour beam. Finally, §4 describes experimental results from the B-III process in a lithium plasma. Simulations are used to explain the experimental results.

2. A single beam

An ultrarelativistic electron beam propagating in an underdense plasma will create a wakefield in the blowout regime [2]. The longitudinal beam slices will experience the focusing force of the positive charge within the blowout, where the envelope of each slice will evolve according to equation [16,17]:

$$\frac{\mathrm{d}^2\sigma_r(z)}{\mathrm{d}z^2} + \left[K_\beta^2 - \frac{\epsilon_N^2}{\gamma_b^2\sigma_r^4}\right]\sigma_r(z) = 0. \tag{2.1}$$

Here, σ_r represent the rms radius of a longitudinal beam slice, $K_\beta = k_p/\sqrt{2\gamma}$ is the betatron wavenumber, $k_p = \omega_p/c$ is the plasma wave number, γ_b is the Lorentz factor for the electron beam and ϵ_N is the normalized emittance. The solution to this equation results in the oscillation of the envelope radius at half the betatron wavelength $\lambda_\beta/2 = \pi/K_\beta$ inside the plasma. As a beam slice reaches the minimum size in the oscillation cycle, the local transverse electric field reaches its maximum value. It is possible to take advantage of this increased field to create a trailing beam via ionization injection. The condition that needs to be satisfied for these electrons to be trapped by the wakefield is given by $\Psi_f = \Psi_i - 1$ [5,7], where $\Psi = (e/mc^2)(\phi - A_z)$ is the normalized value of the wake's effective potential, and subscript 'i' indicates the value of the effective potential at the point of ionization and subscript 'f' at the location of trapping. Here, ϕ is the electric potential and A_z is the longitudinal component of the vector potential. This method for generating trailing beams is called beam-induced ionization injection (B-III).

To illustrate the physics involved in beam generation via B-III, we present the results of a 3D simulation, where the LIT plasma source is the hydrogen gas, which has been preionized before the drive beam arrives. The HIT impurity gas used in these simulations is helium. The hydrogen plasma has a trapezoidal profile with a peak density of $2.5 \times 10^{17}\,\mathrm{cm}^{-3}$. The drive beam parameters used are similar to those that were available at the FACET facility of the SLAC National Accelerator Laboratory, with 20.35 GeV of energy, with an rms longitudinal length of $\sigma_z \sim 30\,\mu\mathrm{m}$ focused to a waist size of $\sigma_r \sim 30\,\mu\mathrm{m}$. The numerical simulation was done with the fully relativistic massively parallel particle-in-cell code OSIRIS [18] in 3D Cartesian geometry. The simulation box was $213^3\,\mu\mathrm{m}^3$ divided into 400^3 cells and followed the beam, moving at speed c longitudinally. To better resolve the beam and plasma evolution, a resolution of 20 cells per skin depth (c/ω_p) or 56 cells per beam size (σ_r/σ_z) were used in the three dimensions. The particle beam and plasma species were initialized with 2^3 macro-particles, representing an ensemble of electrons, per cell. The hydrogen plasma was modelled as a species of free electrons and a fixed background density of ions, starting from 638 μm and linearly reaching the peak density after 1 cm. The helium species was modelled as neutral gas that was ionized according to the OSIRIS Ammosov–Delone–Krainov (ADK) [19] tunnel ionization model. The concentration of helium was 1% of the hydrogen plasma electrons in a 1 cm long section centred 3 cm into the plasma, longitudinally, within two 500 μm long density ramps. The simulation ended after about 6.3 cm.

Figure 1 illustrates the radial oscillation of the longitudinal beam slices and the resulting ionization injection of helium in the wakefield. The drive beam is propagating to the right and creates a wakefield in the hydrogen plasma (hydrogen electrons shown in blue). The radius of

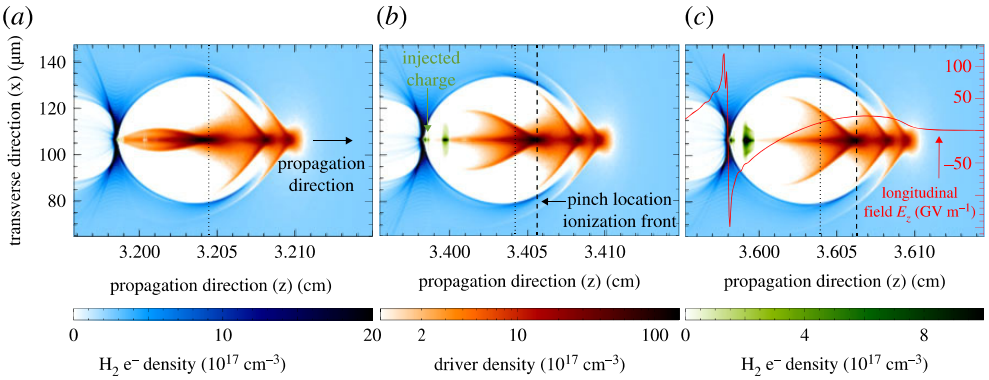


Figure 1. Two-dimensional slices of the three-dimensional simulation showing the betatron oscillation of the drive beam (red colour scale) as it propagates through the plasma (blue). Snapshots (*a–c*) were taken at ct = 3.196, 3.396 and 3.596 cm. The beam propagates from left to right side of plot. Dotted thin lines indicate the pinching location in (*a*). Dashed lines are the pinching location in (*b*) and (*c*). The beam pinch ionizes helium and its electrons (green) are injected in the bubble (white). Plot (*c*) includes the on-axis longitudinal wakefield (red line and axis).

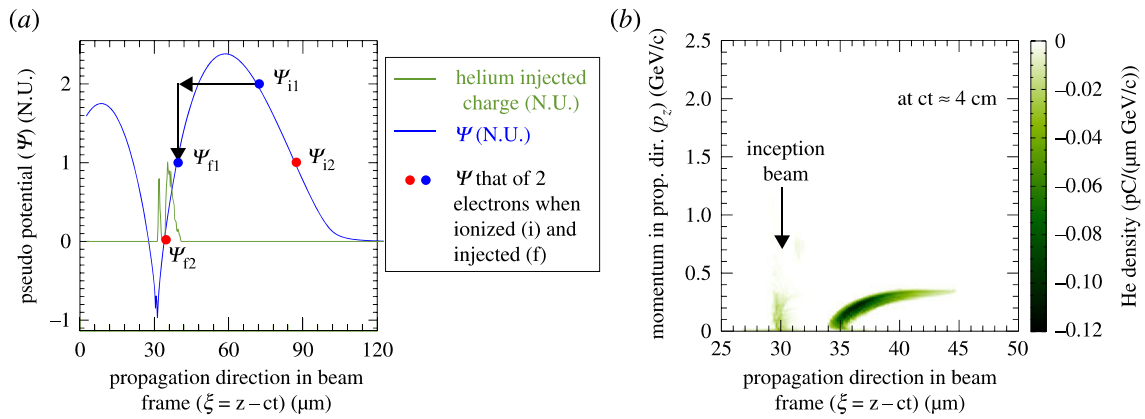


Figure 2. Plot (*a*) shows the normalized pseudo potential, Ψ (blue line) associated with wakefields overlapping the injected helium density (normalized to peak density). Dots represent the initial (i) and final (f) Ψ and ξ positions of two sample electrons. The injected charge longitudinal phase space is depicted in (*b*). The additional beam (marked with an arrow) behind the main trailing beam is called the inception beam and is described in further detail below. Both plots (*a*) and (*b*) refer to ct ≈ 4 cm.

the drive beam slices (orange colour) are seen oscillating in the wakefield. It is important to note that the various longitudinal slices of the drive beam oscillate out of phase, i.e. while some slices are at minimum radial size, others are at their maximum radial size. This is because each slice experiences a different decelerating gradient as well as slightly different plasma density. This out-of-phase oscillation of longitudinal slices results in a distinct 'pinch feature', which moves with respect to the beam along $\xi = \mathrm{ct} - z$. The transverse field at the location of the pinch in the region delineated by two vertical dashed lines in figure 1*c* exceeds the ionization threshold of helium. The slices outside this region do not have enough charge to ionize helium when they pinch.

As the pinch travels forward in the frame of the beam, each slice where the electric field exceeds ionization threshold will generate free electrons. Once these electrons absorb enough energy from the wake, they can then be trapped and injected into the wake. Because of the shape of the Ψ function, electrons ionized by the front-most slices of the beam are injected farthest back in the blowout. Figure 2*a* illustrates this effect for two electrons, where the ionization (i) and injection (f) locations are correlated by the formula $\Psi_f = \Psi_i - 1$ mentioned above.

As the location of ionization (where the pinch is) changes in the frame of the wake, the value of the effective potential varies from Ψ_{i1} to Ψ_{i2}. The electrons released over time will then be distributed along a distance of Ψ_{f1} to Ψ_{f2}. This effect is illustrated in figure 2*b*, where electrons are injected over the range of $32\,\mu\text{m} \leq \xi \leq 45\,\mu\text{m}$. This figure shows the longitudinal phase space for helium electrons corresponding to the instant in time when the electrons ionized by the slice nearest to the front of the drive beam (i.e. $\Psi_i = \Psi_{i2}$ if figure 2) are trapped. Since the pinch moves forward in the frame of the beam, the electrons at the front (higher ξ_i) are ionized and trapped at an earlier time. This variation in injection time in the wakefield results in a natural energy spread in energy from the front to the back.

In summary, ionization injection initiated by the fields of the oscillating electron beam can result in injection of a trailing beam. The longitudinal slices oscillating out of phase create a 'pinch' feature, which moves longitudinally in the frame of the beam. Where the field of the pinch exceeds the ionization threshold of the HIT (helium), these electrons are ionized, and once injected, their final injection phase corresponds to the ionization location via $\Psi_f = \Psi_i - 1$. In the next section, the possibility of generating a multi-coloured bunch will be demonstrated and the injected beams' characteristics will be discussed.

3. Multi-colour beamlets

To inject multiple beamlets using B-III, one could take advantage of the fact that the radial size of each longitudinal slice oscillates with a wavelength of $\lambda_\beta/2$. Therefore, if the length of the HIT region, L_{HIT}, spans multiple lengths of $\lambda_\beta/2$, the number of beamlets, N, is given by

$$N = \frac{L_{\text{HIT}}}{\lambda_\beta/2}. \tag{3.1}$$

In other words, given that the ionized electrons satisfy the trapping condition, one can obtain the same number of bunches as the number of betatron cycles in HIT region. For the plasma density and electron beam parameters presented in the previous section, $\lambda_\beta/2 \sim 1\,\text{cm}$, and therefore the region of helium impurity of 2 cm spans two betatron cycles.

Since the electrons injected at a particular location ξ gain energy from the accelerating field during the span of the betatron oscillation, there is clear separation between individual injected beamlets. This separation in energy can be seen in figure 3*a*, which shows the phase space of the helium electrons for the same simulation set-up as §2 after 5 cm of propagation in plasma. Each of the two oscillation cycles resulted in a clear and distinct beamlet, where the electrons are injected over a very similar range of ξ.

The properties of these beamlets appear in table 1. The charge in each beamlet is slightly lower than 110 pC. Both beamlets have less than 5% energy spread and the emittance of both is about 7 mm-mrad. Additionally, the beamlets are extremely small (approx. 2 μm) in both σ_z and σ_r. From the discussion in §2, σ_z of the injected beam is a function of ξ over which the ionization occurs. Therefore, the size of the injected beamlets can be further reduced by having an impurity region that only covers a fraction of the oscillation cycle length.

The energy difference between the two beamlets can be estimated as the energy an electron in the higher-energy-beamlet gains before the electrons in the lower-energy-beam are injected. The acceleration length is obtained from the envelope oscillation model and the acceleration field from the nonlinear blowout theory [2]. Assuming negligible energy loss for the drive beam during half a betatron oscillation cycle, the acceleration length $d = \lambda_\beta/2 = \pi\sqrt{2\gamma_b}/k_p$ only depends on plasma density through k_p. Meanwhile, the peak 'usable' electric field is given by $eE_z/(mc\omega_p) = \sqrt{n_b/n_p}k_p\sigma_r$. Using these expressions, the energy difference between the two beamlets $\Delta W = eE_z d$ is independent of the plasma density and is therefore only dependent on the drive beam characteristics. For the beam described here, this value is 0.55 GeV, which is in very good agreement with 0.56 GeV given by the simulation. The equation of the electric field given above is the maximum 'usable' field of the unloaded wake. Therefore, the difference between the

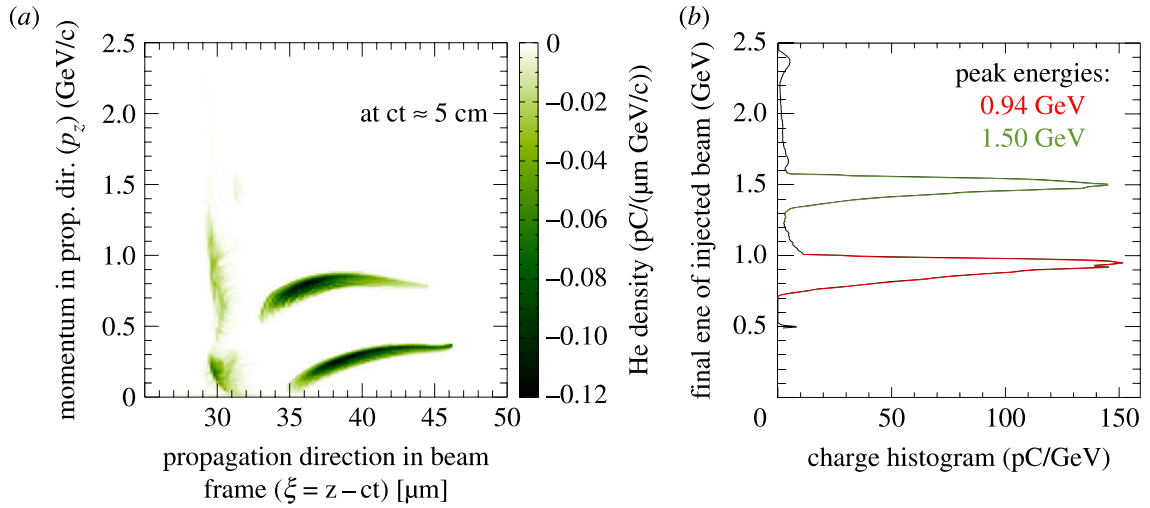


Figure 3. Plot (*a*) contains the longitudinal phase space of injected helium electrons at ct ≈ 5 cm. Plot (*b*) is the histogram of that injected charge after it accelerated, at ct ≈ 6.3 cm. Green colour corresponds to beam injected before ct ≈ 4 cm, shown in figure 2 plot (*b*).

Table 1. Table of results for the multi-colour bunches. The two emittances are the same, as is the sigma.

	Q [pC]	E (rms) [GeV]	$\Delta E/E$ (rms)	ϵ_N [μm]	σ_z [μm]	σ_r [μm]	I_{peak} [kA]
high E	107	1.49	3.1%	7.3	2.3	1.4	5.8
low E	104	0.93	4.8%	6.9	2.7	1.56	4.3

real loaded value of the electric field in the simulation and that calculated from the expression given by Lu *et al*. [2] results in difference between the two fields.

The energy spread of the injected beamlet reduces as it propagates in plasma from 4 to 5 cm. This effect, which can be observed between figures 2*b* and 3, is for two reason: First, the electrons ionized closer to the front of the drive beam (higher ξ value in figure 3) are injected first. Second, the charge of the injected beamlet is not quite enough to flatten the electric field, i.e. beam load the wake [20]. Thus, although the electrons at higher ξ are injected first and therefore have higher energy initially (figure 2*b*), the difference in accelerating gradient between the electrons at the front and at the back of the same beamlet allows the electrons at the back to catch up, resulting in the reduction of energy spread as the beamlets travel 1 cm in plasma.

Ideally, one would be interested in higher injected charge to beam load the wake and further reduce the energy spread. However, the increase in injected beams' charge is accompanied by the injection of a third beam, called the inception beam [21], which in this simulation is visible at $28\,\mu m \leq \xi \leq 33\,\mu m$. This beam, explained in more detail in [21], results from ionization injection due to the field of the injected beamlets. Due to its high energy spread, the energy of the electrons in this third 'inception' beam overlaps with the energy of the electrons from the multi-coloured beamlets. Thus, it will be experimentally very difficult to separate the two. Furthermore, as the charge in the multi-coloured beam increases with higher helium impurity for instance, the charge in the inception beam will also increase. Thus, mitigating this latter effect is an important consideration experimentally for beam-loading the wake.

In summary, extending the region of HIT impurity to multiple betatron envelope oscillation cycles results in the injection of a multi-coloured beam. Although only two beamlets were injected in this simulation, the same principle could be used to inject as many desired bunches by further extending the impurity region. The maximum amount of charge however is limited by the beam-loading considerations, including the avoidance of inception beam.

4. Injecting multiple bunches on the density up ramp of a lithium plasma

In the previous section, we showed how B-III can be used to generate a multi-colour beam in the case where a HIT impurity spans multiple betatron oscillation cycles in a LIT plasma. Lithium plasma is a primary example of a well-characterized plasma source with an HIT impurity region, which spans several betatron wavelengths. This plasma source consists of a heat pipe oven [22], where solid lithium is heated beyond the melting point. The resulting liquid lithium creates a vapour pressure, which at equilibrium creates a nearly uniform density. At the boundaries of the hot lithium vapour, cold helium is used to spatially contain the vapour within the heat pipe oven. Therefore, in the region of overlap, a lithium density up ramp is created, which is accompanied by a helium density down ramp. An example of the measured density profile is shown in figure 4.

This plasma source was used for PWFA experiments at the FACET. The FACET electron beam containing 3.2 nC of charge and 20.35 GeV of energy was focused to a σ_r of 30 μm in the middle of the lithium density up ramp. The nominal beam length was $\sigma_z \sim 30\,\mu$m. The field of the FACET beam at waist was sufficient to ionize the lithium (LIT element), but not helium (the HIT element). Since helium spanned nearly 10 cm, a multi-coloured beam was expected from the beam-induced ionization injection of helium electrons in the wakefield driven in the lithium plasma.

In the E217 experiments with the lithium plasma at FACET, a series of datasets, each containing 50 shots, were sequentially recorded at 1 Hz. The variation in these results was the consequence of the natural shot-to-shot jitter in the electron beam properties. The lithium vapour source itself was very stable on the time scale of the datasets. The main diagnostic in these experiments was an imaging magnetic spectrometer [24], which contained a dipole and two quadrupoles. The dipole dispersed electrons by energy, while the quadrupole pair allowed for imaging of electrons at a particular energy. There were two particular datasets where the spectrometer results oscillated between showing no injected electron beams to injected electron beams with over 10 GeV of energy and a wide energy spread. Such shot-to-shot variation indicated that the drive beam's properties were at the threshold of enabling the B-III process.

Three sample data representing the range of possibilities for the injected electron spectra are presented in figure 5, ordered in increasing drive beam current from 5*a* to *c*. The relative drive beam current is deduced in two ways. First, by comparing the signal from a pyroelectric detector (pyro), and second by comparing the energy loss of the drive beam, for each shot. The signal from the pyro, which is progressively higher for figure 5*a*–*c*, is inversely correlated with σ_z [25,26]. The energy loss is measured from the initial energy (20.35 GeV) to the lowest energy reached by the electrons in the drive beam. This is clearly marked for figure 5*a*, where both the initial and final energy of the electrons are visible. The energy range in figure 5*b* and *c* is confined to the values between approximately 8 and 13 GeV to more clearly show the trailing beams. The trailing beams in these figures can be clearly distinguished from the electrons in the drive bunch because they have a much lower emittance than the drive bunch [12]. Therefore, trailing beams appear transversely narrower on the spectrometer. The electrons in the drive beam reach progressively lower energies in the data shown from 5*a* to *c* as indicated by the dashed line in these figures. This increase in the energy loss for the drive beam electrons indicates the formation of a more nonlinear wake, which is the second evidence for the beam current increasing from figure 5*a* to *c*.

The data shown in figure 5 indicate that the energy spectrum of the trailing beam varies with the driver beam current. At the highest current in the dataset, a trailing beam with a wide energy spread that covered the entire range of the beam's energy is observed (figure 5*c*). At the lowest current (figure 5*a*), no trailing beams were observed. In 10% of the experimental shots, where the drive beam's current is intermediate (represented by figure 5*b*), beams with up to 5 distinct beamlets were observed.

The energy separation between the beamlets observed in figure 5*b* is between 0.3 and 0.4 GeV. However, it must be noted that the signal to noise ratio is not uniform on the spectrometer for all electrons. In particular, the signal to noise ratio of the electrons on the spectrometer is a function of the betatron phase at which they leave the plasma [27]. Therefore, there might be a slight shift

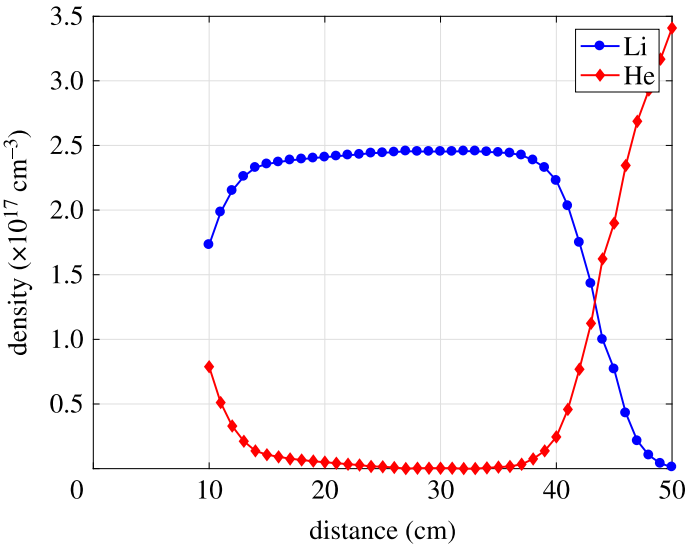


Figure 4. Density profile of helium and lithium along the heat pipe oven in E217 experiment at FACET. The individual data points are deduced from the experimentally obtained measurements of lithium temperature and temperature pressure curves [23]. Lines are used to interpolate values between the experimentally measured data.

and distortion in the peak energy of the beamlets observed in the experiment. The fact that this effect is not observed in figure 5*c* indicates that it is not dominant in the interaction under study.

We explored the B-III process at the threshold of beam generation through OSIRIS simulations in 2D cylindrical geometry. In addition to observing the variation in the physical processes involved (i.e. ionization and injection), a primary goal was to investigate the properties of the injected beam across this threshold to observe whether a beam with multi-coloured features similar to experiment emerged (due to multiple injection cycles) from this process. Simulations were performed with the drive beam parameters being mostly the same as those described in §2, except σ_z was varied between 30 µm to 60 µm. The threshold of injection was observed to occur with $\sigma_z \sim 40$ µm. The three simulations near the threshold effect, i.e. for $\sigma_r = 30$, 40 and 45 µm used 1560×450, 720×270 and 1630×450 cells in 234, 255 and $271 \times 96\ \mu m^2$ to ensure that the different beams were captured and resolved correctly. The plasma was initialized with 4×4 macro-particles per cell and the beam with 2×2. The lithium profile started 3.5 µm after the simulation box and its density grew linearly for 10 cm and reached a constant plateau, whilst the helium density decreased and vanished. The mixture of lithium and helium was initialized as neutral species, ionized according to the ADK model, except for the run with the 45 µm beam, where lithium was assumed to be pre-ionized and radially uniform to provide more stable wake evolution along the lithium density up ramp (to prevent loss of injected electrons). The concentration of helium was 100% for the 45 µm beam (to maximize ionization and hence injection probability) and 20% for the other two runs. The code modelled the two electron energy levels of helium separately and we observed that the core electron corresponded to a low percentage of the injected charge. All simulations reached 20 cm into the plasma. This length is shorter than the plasma length in the experiments. This is because a large amount of charge is injected in these simulations, which makes them very computationally demanding.

Both processes, i.e. ionization due to the drive beam pinching and the injection of ionized electrons, were observed to be at the threshold for this range of beam properties. In figure 6*a–c*, it can be seen that the ionization fraction drastically decreased as σ_z was changed from 35 to 45 µm. When σ_z was increased to 60 µm, the transverse field due to pinching of the beam ceased to ionize helium all together. This is because at higher σ_z values, the beam charge gets distributed over a larger range, and therefore the field of the pinch is not as high as the case with smaller σ_z.

The threshold effect of injection can be observed in figure 6*d–f*, where the density of the helium electrons near the axis (green contour) is shown overlapping with the value of Ψ (red and blue

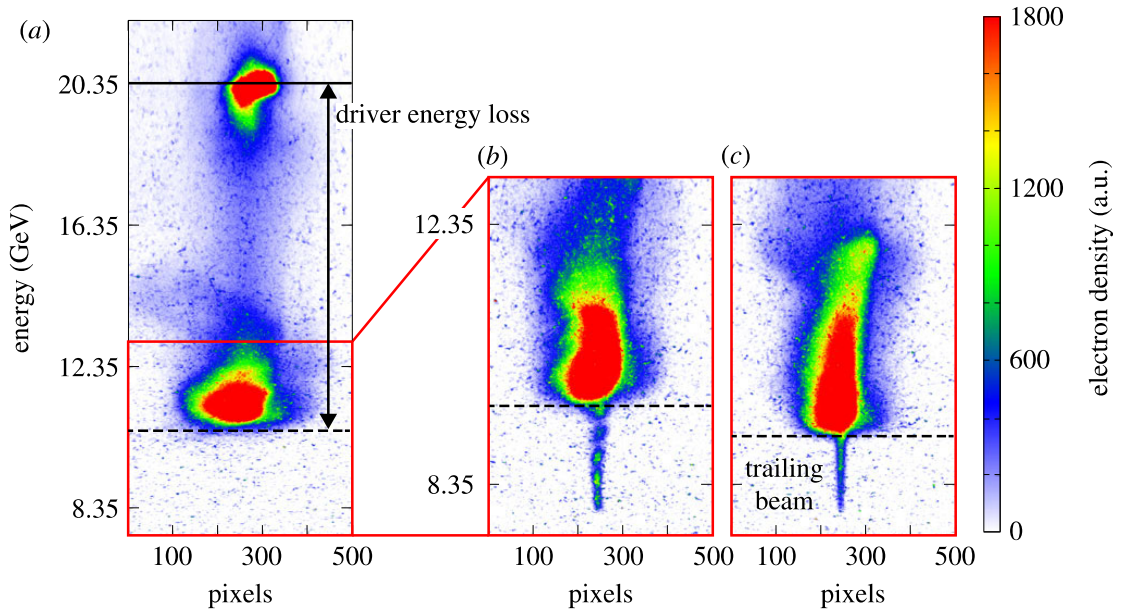


Figure 5. Results from FACET E217 experiments. The spectrometer images are shown for three representative results from the interaction of the FACET beam with the lithium source in figure 4. The initial beam energy was at 20.35 GeV marked by solid black line in (*a*). Quadrupole setting selected to focus electrons at 8.35 GeV. Energy range for (*b*) and (*c*) is changed to 8–13 GeV to better show the features of the injected charge in the region of interest. (*a*) A case where only the energy loss of drive beam electrons (down to approx. 10 GeV) is observed. (*b*) A case where a narrow beam is observed between 8 and 10 GeV in addition to the energy loss of the drive beam electrons (energy larger than 10 GeV). Clear multiple peaks appear within the narrower lower energy beam. (*c*) A third case where the narrow beam injected below the drive beam electrons has a continuous energy spread, as opposed to the clear features in (*b*). Lowest energy reached by the electrons of the drive beam is marked by a black dashed line.

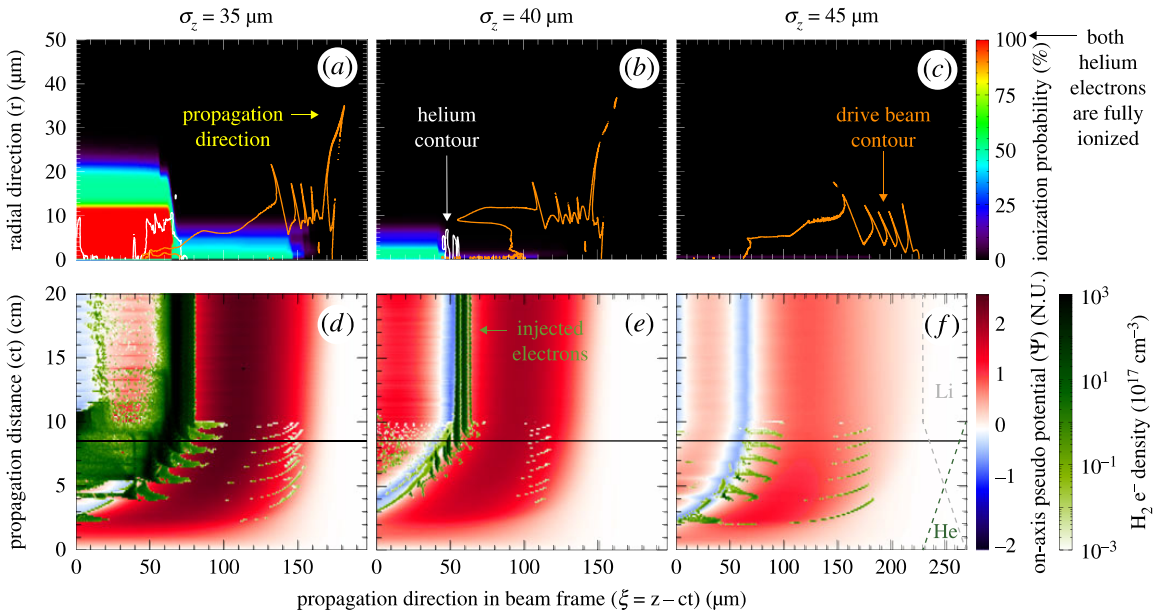


Figure 6. Helium ionization probability (top row, (*a–c*) plots) for the simulations with drive beam with $\sigma_z = 35$ (*a,d*), 40 (*b,e*) and 45 μm (*c,f*) at propagation distance ct = 8.5 cm. Superposed are the density contours of 10^{17} cm^{-3} for the drive beam (orange) and helium injected charge (white). The ionization probability of 50% (100%) indicates full ionization of the outer (inner) helium electron. The bottom row shows the evolution in time, ct of the pseudo potential (red/blue), Ψ, and helium density (green) close to the axis for those simulations. Solid lines are at ct = 8.5 cm. Dashed lines indicate the longitudinal profile of the lithium (grey) and helium impurity (green) neutral gases.

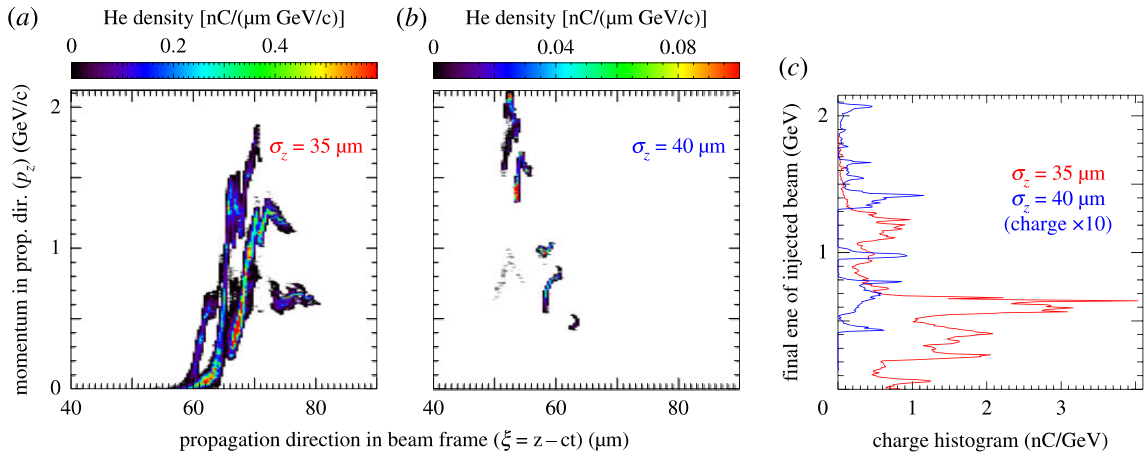


Figure 7. Longitudinal phase space of the injected helium for the simulations with $\sigma_z = 35$ (*a*) and 40 μm (*b*) 1 cm after the end of the helium down ramp, at ct = 11 cm. Plot (*c*) shows the spectra of both simulations, 35 (red) and 40 (blue) μm, at the same time. The charge was increased by a factor of 10 for the 40 μm run (blue).

contour). The expected number of oscillations for the beam envelope is seven according to the numerical solution to equation (2.1). This is the same as the helium ionization events (green colour, e.g. figure 6*f*) observed in the up ramp of the lithium plasma (grey dashed line). The electrons injected in the first few cycles however get ejected from the blowout region as the plasma density increases. This is because as the lithium density increases in the ramp, the blowout region becomes shorter. The number of ionization events due to pinching represents the upper bound on the number of final beamlets expected in this experiment. As will be discussed below, only five beamlets are observed to remain trapped in the simulation, in agreement with the number of beamlets observed in the experiments (e.g. figure 5).

The reduction in the size of the blowout region is shown in the Ψ contour by the blue colour (representing the back of the bubble) moving closer to the beam front at higher *ct*. Early in the ramp, the charge is injected too far back in the wakefield and as the bubble gets shorter, the back of the bubble where the electron sheaths cross overtakes the injected charge. Since the transverse field at that point in the bubble is strongly defocusing, the helium charge gets ejected transversely from the bubble. In the $\sigma_z = 40\,\mu$m case, for example (figure 6*e*), several beamlets injected early (green colour, ct $\sim 5 - 8$ cm) are ejected once the back of the bubble moves forward towards $\xi \sim 50\,\mu$m. However, if the amount of the injected charge is too large, the force exerted by them on the sheath electrons pushes the trajectory of sheath electrons backwards in the frame of the drive beam. Although this effect is more difficult to see in these figures, it occurs for the case of $\sigma_z = 35\,\mu$m (figure 6*d*) after ct ~ 8 cm. From that point on, the back of the bubble does not move forward to larger values of ξ.

The charge ionized and injected in the $\sigma_z = 35\,\mu$m and $\sigma_z = 40\,\mu$m simulations in the ramp of the lithium plasma remain in the blowout after the ramp region. This is not the case for the $\sigma_z = 45\,\mu$m simulation. Although some charge is initially injected in the latter case, those electrons overlap with the electrons of the drive beam. The transverse fields due to the betatron oscillation of the drive beam slices are strong enough to transversely eject the newly injected helium electrons. Therefore, no charge remains in the case of $\sigma_z = 45\,\mu$m after the up ramp section (ct ~ 10 cm). While the peak values of Ψ decrease as σ_z increases (i.e. current decreases) in figure 6*d–f*, the reduction in Ψ is not the primary reason for the absence of the injected beam in the $\sigma_z = 45\,\mu$m simulation.

The longitudinal phase space of the injected electrons 1 cm after the plasma ramp is shown in figure 7. Five distinct beamlets are observed in this phase space in figure 7*b*. Each of these beamlets gets injected during a distinct betatron cycle, and the lower energy ones are injected at a later time. This is because the increased density in the lithium up ramp leads to higher fields, and

therefore higher peak values of Ψ (both positive and negative) within the blowout region. Because the peak values of Ψ is increasing, electrons ionized in the later cycles of betatron oscillation are trapped closer to the front of the blowout regime (higher ξ values in figure 7). The $\sigma_z = 40\,\mu\text{m}$ results represent the near-threshold results similar to the experimental results in figure 5*b*.

Multiple beamlets injected over several betatron oscillations are also observed in the case of $\sigma_z = 35\,\mu\text{m}$ (figure 7*a*). However, (partially) due to the increased ionization fraction in this case, the wakefield is over loaded. Therefore, while the beamlets injected at the latest time $75\,\mu\text{m} < \xi < 80\,\mu\text{m}$ and $p_z \sim 0.6\,\text{GeV c}^{-1}$ appear to have fairly low energy spread, the other two beamlets have very high energy spread. This is because the back part of these beamlets is in the over-loaded regime and is seeing a lower accelerating field than the front part. This high energy spread can be seen in the histogram of the two spectra (figure 7*c*, red contour), where the overlapping energies of the different beamlets contribute to a large energy spread. This observation is also very similar to figure 5*c*, which shows a background charge with wide energy spread and peaks overlaid on top of it.

The energy separation between the beamlets in the simulation with $\sigma_z = 40\,\mu\text{m}$ after propagating 1 cm in the plateau is around 0.4 GeV (see blue curve in figure 7*c*). In comparison, the experimental separation between the beamlets in figure 5*b* is around 0.3 GeV. The separation between beamlet energies immediately after the helium region is on the same scale for experiment and simulation. In the region after, the accelerating field is much higher in the simulations than would be implied by the experimental results. This difference is primarily due to the deviation of the beam current profile in the experiment from an ideal Bi-Gaussian, which was the profile applied in the simulations. The beam properties varied from shot to shot and are not known with great precision. In this sense, the one to one comparison of the final simulation spectra with the experiment for the trailing beam is not meaningful. However, there is a clear similarity in the key features of the electron energy spectra between the simulation and the experiment. These features include the threshold behaviour for the appearance of injected charge, the transition from multi-colour beamlets to a beam with wide energy spread, and the trend of these effects as the beam current is increased, i.e. σ_z is decreased. These are evident in the similarities between figure 7*b* and 5*b* showing multiple beamlets and the similarity between 7*a* and 5*c*, showing a continuous energy spread (with higher charge at higher energy) as well as the number of injected beamlets.

In summary, helium injected charges exhibiting distinct energy features were observed in the experiment. Such beam characteristics appeared at the threshold of beam generation. We know this because the results oscillated between no injected charge and injected charge with large energy spread, indicating that for the distinct energy features to appear, conditions had to be optimal. Simulations of the FACET beam propagating in the lithium plasma source emphasized the importance of both ionization and injection at the threshold of beam generation. Parameter scan around the threshold of injection revealed final spectra that shared similar characteristics as those observed in the experiment: when $\sigma_z = 45\,\mu\text{m}$, no beam was injected, when $\sigma_z = 40\,\mu\text{m}$ the spectra exhibited distinct peaks associated with multiple injected beamlets, and when $\sigma_z = 35\,\mu\text{m}$, the overloading of the wake due to increased ionized and injected charge, resulted in large energy spread for the injected beamlets, which created a final spectra with large energy spread.

5. Conclusion and future work

In this paper, we discussed the generation of a multi-coloured beam as a unique application of the beam-induced ionization injection (B-III) in a plasma wakefield accelerator. This technique relies on the periodic envelope oscillation of a mismatched drive beam in plasma made from a mixture of a LIT plasma source and an extended region of an HIT impurity. The periodic ionization and injection of the HIT element can lead to a beam containing overlapping low energy spread beamlets centred at different energies.

Simulations of the lithium plasma showed that injection of multiple beamlets is possible at the threshold of beam injection, which was suggested by the FACET E217 experimental results. Because of the lithium density up ramp and the helium density down ramp, several of the

beamlets initially injected were actually ejected from the wake, and furthermore, those injected had varying characteristics, and were injected at different locations of the wake. To obtain beamlets with consistent characteristics, a different plasma source is needed. The new plasma source needs to have an uniform-density LIT gas imbedded with an HIT impurity with adjustable length and characteristics. Such a plasma source will allow for clear demonstration of multi-coloured beam generation in a PWFA. Moreover, the proper design of the helium impurity region paves the way for generating beams with tailored density characteristics, as well as a careful investigation of the effect of beam loading on the injected beam.

Data accessibility. The data that support the findings of this study are available from the corresponding author upon request.

Competing interests. The authors declare that they have no competing interests.

Funding. Work at LOA was supported by the European Research Council (M-PAC project, Contract No. 715807). Simulations were performed on the UCLA Hoffman2 cluster through NSF OCI-1036224. Work at UCLA was supported by DOE Contracts No. DE-SC0010064, No. DE-SC0008491, No. DE-SC0008316 and NSF Contracts No. PHY-1415386, No. PHY-1734315, No. ACI-1339893, No. PHY-0960344. Work at SLAC was supported by DOE Contract No. DE-AC02-76SF00515.

References

1. Rosenzweig JB *et al.* 1991 Acceleration and focusing of electrons in two-dimensional nonlinear plasma wake fields. *Phys. Rev. A* **44**, R6189–R6192. (doi:10.1103/PhysRevA.44.R6189)
2. Lu W *et al.* 2006 Nonlinear theory for relativistic plasma wakefields in the blowout regime. *Phys. Rev. Lett* **96**, 165002. (doi:10.1103/PhysRevLett.96.165002)
3. Blumenfeld I *et al.* 2007 Energy doubling of 42 GeV electrons in a metre-scale plasma wakefield accelerator. *Nature* **445**, 741–744. (doi:10.1038/nature05538)
4. Litos M *et al.* 2014 High-efficiency acceleration of an electron beam in a plasma wakefield accelerator. *Nature* **515**, 92–95. (doi:10.1038/nature13882)
5. Oz E *et al.* 2007 Ionization-induced electron trapping in ultrarelativistic plasma wakes. *Phys. Rev. Lett.* **98**, 084801. (doi:10.1103/PhysRevLett.98.084801)
6. Kirby N *et al.* 2009 Transverse emittance and current of multi-GeV trapped electrons in a plasma wakefield accelerator. *Phys. Rev. ST Accel. Beams* **12**, 051302. (doi:10.1103/PhysRevSTAB.12.051302)
7. Pak A *et al.* 2010 Injection and trapping of tunnel-ionized electrons into laser-produced wakes. *Phys. Rev. Lett.* **104**, 025003. (doi:10.1103/PhysRevLett.104.025003)
8. McGuffey C *et al.* 2010 Ionization induced trapping in a laser wakefield accelerator. *Phys. Rev. Lett.* **104**, 025004. (doi:10.1103/PhysRevLett.104.025004)
9. Hidding B *et al.* 2012 Ultracold electron bunch generation via plasma photocathode emission and acceleration in a beam-driven plasma blowout. *Phys. Rev. Lett.* **108**, 035001. (doi:10.1103/PhysRevLett.108.035001)
10. Li F *et al.* 2013 Generating high-brightness electron beams via ionization injection by transverse colliding lasers in a plasma-wakefield accelerator. *Phys. Rev. Lett.* **111**, 015003. (doi:10.1103/PhysRevLett.111.015003)
11. Martinez de la Ossa A *et al.* 2013 High-quality electron beams from beam-driven plasma accelerators by wakefield-induced ionization injection. *Phys. Rev. Lett.* **111**, 245003. (doi:10.1103/PhysRevLett.111.245003)
12. Vafaei-Najafabadi N *et al.* 2016 Evidence for high-energy and low-emittance electron beams using ionization injection of charge in a plasma wakefield accelerator. *Plasma Phys. Control. Fusion* **58**, 034009. (doi:10.1088/0741-3335/58/3/034009)
13. Hidding B *et al.* 2014 Tunable electron multibunch production in plasma wakefield accelerators. (http://arxiv.org/abs/1403.1109v1 [physics.plasm-ph]).
14. Zeng M *et al.* 2015 Multichromatic narrow-energy-spread electron bunches from laser-wakefield acceleration with dual-color lasers. *Phy. Rev. Lett.* **114**, 084801. (doi:10.1103/PhysRevLett.114.084801)
15. Hogan MJ *et al.* 2010 Plasma wakefield acceleration experiments at FACET. *New J. Phys.* **12**, 055030. (doi:10.1088/1367-2630/12/5/055030)

16. Clayton CE *et al.* 2002 Transverse envelope dynamics of a 28.5-GeV electron beam in a long plasma. *Phys. Rev. Lett.* **88**, 154801. (doi:10.1103/PhysRevLett.88.154801)
17. Marsh KA *et al.* 2005 Beam matching to a plasma wake field accelerator using a ramped density profile at the plasma boundary. In *Proc. PAC 2005* 2702.
18. Fonseca RA *et al.* 2002 OSIRIS: a three-dimensional, fully relativistic particle in cell code for modeling plasma based accelerators. *Lect. Notes Comput. Sci.* **2331**, 342. (doi:10.1007/3-540-47789-6)
19. Ammosov MV, Delone NB, Krainov VP. 1986 Tunnel ionization of complex atoms and of atomic ions in an alternating electromagnetic field. *Sov. Phys. JETP* **64**, 1191–1194. (doi:10.1117/12.938695)
20. Tzoufras M *et al.* 2008 Beam loading in the nonlinear regime of plasma-based acceleration. *Phys. Rev. Lett.* **101**, 145002. (doi:10.1103/PhysRevLett.101.145002)
21. Amorim LDA, Vafaei-Najafabadi N. 2018 Narrow 'inception' beams generated in FACET beam-driven wakefield accelerator setups. In *Proc. AAC 2018*, accepted.
22. Muggli P *et al.* 1999 Photo-ionized lithium source for plasma accelerator applications. *IEEE T. Plasma Sci.* **27**, 791–799. (doi:10.1109/27.774685)
23. Mozgovoi AG *et al.* 1987 The saturated vapour pressure of lithium, sodium, potassium, rubidium, and cesium. *High Temp.-High Press.* **19**, 425–430.
24. Adli E *et al.* 2015 Cherenkov light-based beam profiling for ultrarelativistic electron beams. *Nucl. Instrum. Meth. A* **783**, 35–42. (doi:10.1016/j.nima.2015.02.003)
25. Vafaei-Najafabadi N *et al.* 2014 Beam loading by distributed injection of electrons in a plasma wakefield accelerator. *Phys. Rev. Lett.* **112**, 025001. (doi:10.1103/PhysRevLett.112.025001)
26. Lipkowitz N, Decker FJ, Sheppard J, Weathersby S, Wienands U, Woodley M, Yocky GS. 2012 Longitudinal beam tuning at FACET. In *Proc. of IPAC 2012, New Orleans, Louisiana*, TUPPC052.
27. Clayton CE *et al.* 2016 Self-mapping the longitudinal field structure of a nonlinear plasma accelerator cavity. *Nat. Commun.* **7**, 12483. (doi:10.1038/ncomms12483)